Supporting Information

Untangling Structure and Dynamics of Lithium-Rich Anti-Perovskites Envisaged as Solid Electrolytes for Batteries

Isabel Hanghofer[§], Günther J. Redhammer[§], Sebastian Rohde[§], Ilie Hanzu[§], Anatoliy Senyshyn[|], H. Martin R. Wilkening[§,*], and Daniel Rettenwander[§,*]

[§]*Graz University of Technology, Institute for Chemistry and Technology of Materials, and Christian Doppler Laboratory for Lithium Batteries Stremayrgasse 9, A-8010 Graz, Austria.*
[$]*University of Salzburg, Department of Chemistry and Physics of Materials, 5020 Salzburg, Austria.*
[|]*Heinz Maier-Leibnitz Zentrum (MLZ), Technische Universität München, 85748 Garching, Germany*

Table S1. Reports on Li-rich anti-perovskite phases published so far and the degree of experimental evidence

Compound (nominal)	Phase behavior	Methode (grade of evidence)	Reference
$Li_2(OH)Cl$	-	Thermochemical investigations (1)	[1]
$Li_2(OH)Cl$	-	Thermochemical investigations (1)	[2]
$Li_2(OH)Cl$	295 K: orthorhombic *Pmma;* $a = 7.680(8)$, $b = 4.001(7)$, $c = 3.899(6)$	Rietveld refinement on PXRD data, phase purity of the samples (4)	[3]
$Li_2(OH)Cl$	<57 °C: orthorhombic SG *Amm*2; $a = 3.8220(1)$, $b = 7.9968(2)$ $c = 7.7394(2)$ >57 °C: cubic SG; *Pm*-3*m* $a = 3.9103(1)$	Rietveld refinement of NPD, and SCXRD data combined with NMR data, phase purity of the samples (5)	[4]
$Li_2(OH)Cl$	<35 °C: orthorhombic SG *Amm*2 >35 °C: cubic SG *Pm*-3*m*	PXRD without refinement data, pattern similar to previous reports (3)	[5]
$Li_2(OH)Cl$	< 35 °C: orthorhombic SG $Pmc2_1$; $a = 3.8749(8)$, $b = 3.8257(8)$, $c = 7.999(1)$ >35 °C: cubic SG *Pm*-3*m* $a = 3.9345(1)$	Rietveld refinement on PXRD data (4)	[6]
$Li_2(OH)_{1-x}FCl_x$	with F: cubic without F: orthorhombic	PXRD, adding LiF leads to an increase of the LiCl reflexions in the PXRD pattern	[7]
$Li_2(OH)Cl$	<35 °C: orthorhombic SG *Amm*2; $a = 3.8220(1)$, $b = 7.9968(2)$ $c = 7.7394(2)$ >35 °C: cubic SG *Pm*-3*m*; $a = 3.9103(1)$	PXRD without refinement, Composition determined by ICP-OES	[8]
$Li_{2.17}(OH_{0.83})Cl$	tetragonal (<-60 °C) SG unknown cubic (> −60 °C) *Pm*-3*m*; a = 3.9135(1)	PXRD without refinement, Composition determined by ICP-OES	[8]
$Li_{1.16}(OH_{1.84})Cl$	cubic, SG *Pm*-3*m* $a = 3.9103(1)$	PXRD without refinement, Composition determined by ICP-OES	[8]
$LiCl \cdot H_2O$	orthorhombic, SG *Amm*2; $a = 7.65884(5)$, $b = 7.73813(4)$, $c = 7.67267(5)$	SCXRD and PXRD with Rietveld refinement	[9]

$Li_4(OH_3)Cl$	monoclinic, SG $P2_1/m$; a = 5.4096(8), b = 7.382(2), c = 6.2076(8), β = 94.40(1)°	SCXRD, first definitive report on this phase – proposed to be the composition previous reported as Li5(OH)2Cl3	[3]
$Li_5(OH)_2Cl_2$	-	PXRD without refinement, analysis was not possible due to the high amount of reflections, assuming its existence	[10]
$Li_5(OH)_3Cl_2$	-	PXRD without refinement, assuming its existence. LiCl reflection increase in the pattern with increasing amount of LiCl in the starting material.	[5]
$Li_3(OH)_2Cl$	-		
$Li_5(OH)_2Cl_3$	-		
$Li_3(OH)Cl_2$	-		
Li3OCl	RT: *Pm*-3*m* DSC: phase changes at 40 °C > 40 °C - tetragonal or orthorhombic	PXRD w.r.	[11]
Li_3OCl	cubic, *Pm*-3*m*: a = 3.91 Å	PXRD without refinement	[12]
$Li_{2.99}Ba_{0.005}OCl_{1-x}(OH)_x$	-	PXRD No refinement, Amount of Li5(OH)2Cl3; at 25◦C after the glass has been conditioned	[12]
$Li_{3-2x}M_xXO$ (M=Mg, Ca)	-	PXRD No refinement	[12]

Table S2: Typical bond lengths in compounds with $Pm\bar{3}m$ and *Pban* symmetry as determined from PND data at 300 K and 4 K

Sample/ T (K)	LRAP_1, 300K	LRAP_3, 4K	LRAP_3, 300K	LRAP_2, 300K
SG	$Pm\bar{3}m$	*Pban*	*Pban*	*Pban*
Li1-O1 x2 (Å)	1.9467(9)	2.0014(5)	2.0244(9)	2.0233(8)
Li1-Cl1 x2 (Å)	2.7531(6)	2.621(6)	2.511(4)	2.515(4)
Li1-Cl2 x2 (Å)	2.7531(6)	2.771(7)	2.951(5)	2.948(4)
Volume (Å^3)	19.67	19.35	19.76	19.77
OQE	1.0499	1.0394	1.0557	1.0553
OAV	0.0	5.3442	43.50	42.10
Li2-O1 x2 (Å)	--	1.9514(18)	1.938(3)	1.940(8)
Li2-Cl1 x2 (Å)	--	2.521(7)	2.73(8)	2.71(12)
Li2-Cl2 x2 (Å)	--	2.995(9)	2.80(8)	2.83(12)
Volume(Å^3)	--	19.35	19.76	19.77
OQE	--	1.0716	1.0539	1.0543
OAV	--	53.46	3.48	5.39
Li3-O1 (Å)	--	1.93(3)	1.768(19)	1.66(2)
Li3-O1 (Å)	--	2.11(3)	2.236(19)	2.26(2)
Li3-Cl2 (Å)	--	2.618(13)	2.36(7)	2.44(7)
Li3-Cl1 (Å)	--	2.124(13)	2.50(7)	2.62(7)
O1-H1 (Å)	0.863(5)	0.864(8)	0.814(11)	0.938(15)
O1-H2 (Å)	--	0.845(8)	0.937(12)	0.883(16)

Polyhedral volume, octahedral quadratic elongation (OQE) and octahedral angle variance (OAV) were calculated using VESTA.

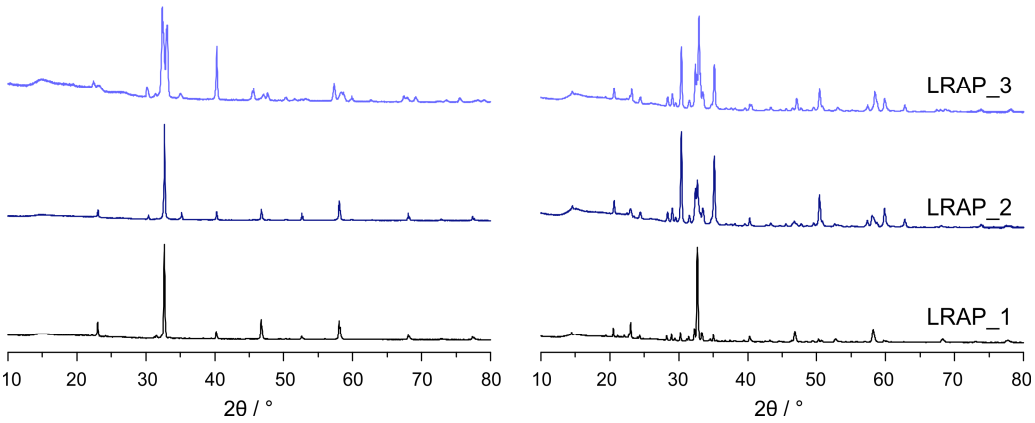

Figure S1. PXRD patterns of LRAP_1, LRAP_2, and LRAP_3, respectively, either recorded before (left) or after (right) the neutron diffraction measurements.

Model finding and refinement of structure

For $Li_2(OH)Cl$ different crystallographic settings are reported in literature: cubic, tetragonal and several orthorhombic unit cells (see Table S1). Indexing of the neutron diffraction data (300 K) of $Li_2(OH)Cl$ (sample LRAP_3) using EXPO2014[15] yields an orthorhombic cell with a = 7.74574(15) Å, b = 7.99730(15) Å and c = 3.82298(7) Å as the best matching model. This corresponds to a 2a, 2b, c setting as compared to the cubic $Pm\bar{3}m$ cell of "Li_3OCl". Using the above mentioned orthorhombic unit cell parameters, all, except two low intensity Bragg peaks at 36.7° 2θ (d = 2.45 Å) and 49.4° 2θ (d = 1.852 Å) could be indexed and refined down to low reliability values. Space group tests on the extracted intensity data were performed using JANA 2006[16], yielding a primitive unit cell with the most probable space group symmetry being *Pbna*. However, it should be noted that also good pattern matching (Le-Bail fits) refinements of data with different space groups could be achieved, using e.g. *Amm*2[8], *Pmma*, *Pmm*2, or *Pmmm* space group symmetry, while *C*-, *F*- or *I*- centered orthorhombic cells do not work at all. Metrics with larger or smaller unit cell parameters were also tested and good matching results are given in Table S3, the results for the different refinements are displayed in Figure S2.

Table S3: Lattice parameters and R_{wp} values, obtained from Le Bail fits with different lattice parameter and symmetry settings to the data of sample LRAP_3 collected at 300 K.

SG	a (Å)	b (Å)	c (Å)	R_{wp}	Reference
*I*4/*mcm*	5.4402(6)	= a	7.9912(14)	7.28	this study
$P4_2/nmc$	7.7806(9)	= a	7.5826(11)	7.07	Weiss *et al.*
*P*4/*mmm*	3.8472(4)	= a	3.9957(7)	6.98	this study
Pmma	7.64582(19)	3.99937(1)	3.87312(9)	2.41	[3]
$Pmc2_1$	3.99923(10)	3.87315(9)	7.64625(18)	2.42	[6]
*Amm*2	3.82317(8)	7.99808(13)	7.74604(16)	2.17	[4]
Pban	7.74574(15)	7.99730(15)	3.82298(7)	1.97	this study
Pmmm	7.74594(15)	7.99645(18)	3.82293(7)	1.91	[18]
Cmcm	7.74644(17)	7.64547(15)	7.9956288(17)	2.12	[19]

Good fits to the data can be achieved with the orthorhombic setting according to ref. 19, *i.e.*, with 2a, 2b, 2c body centred cell *w.r.t.* the cubic cell. However, it is also evident that tetragonal cells do not fit adequately our experimental data at room temperature. To conclude, based on pure Le-Bail fits alone, it is not possible to decide for the correct unit cell and structural setting. Thus, in the next step, using the *Cmcm*, *Pmmm*, *Pmm*2 and *Pban* symmetry, complete structure solutions were conducted. The *Amm*2 space group model was dismissed as analysis of intensity statistics clearly indicated a primitive unit cell for the 2a, 2b, c setting (see above) and first structure solutions did not yield sufficient acceptance at all.

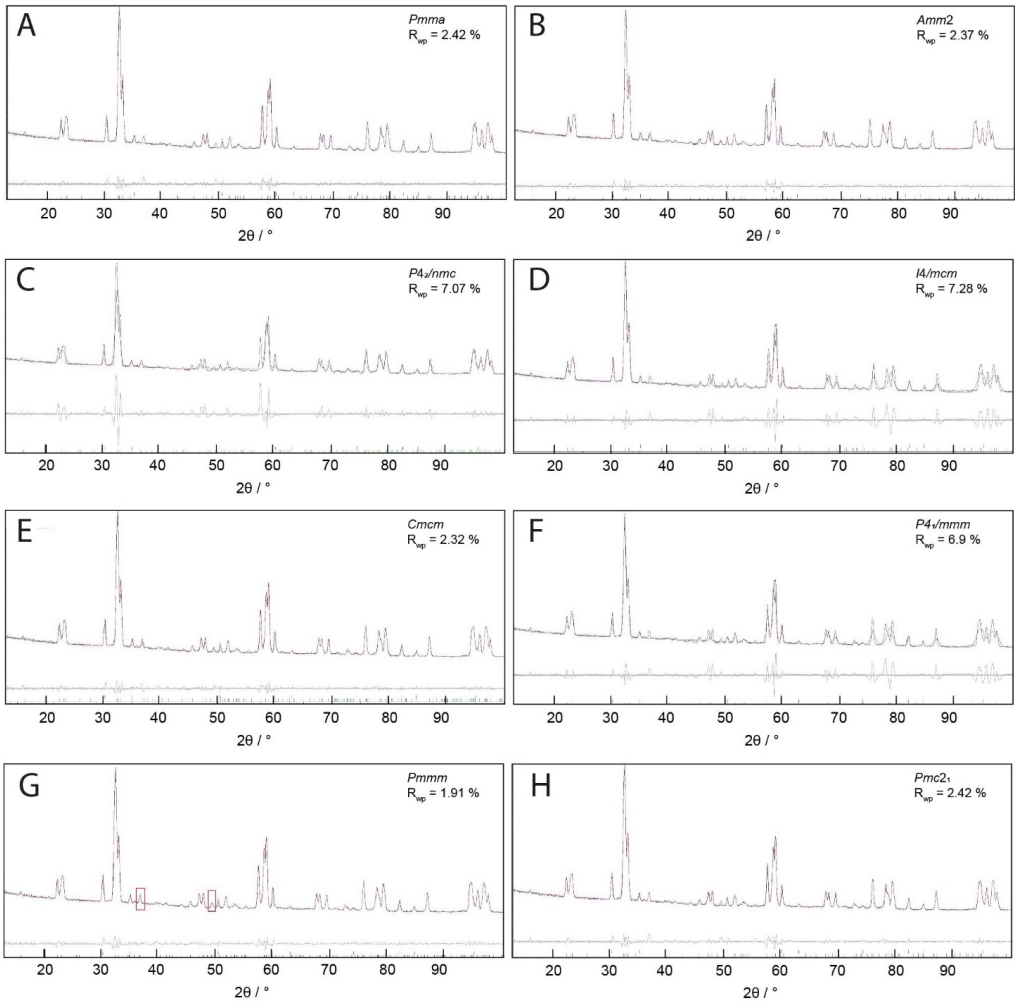

Figure S2: Sections of the diffraction pattern of LRAP_3 at 300 K; the patterns were fitted to different crystallographic settings using Le-Bail refinements, *i.e.*, without a structural model.

In structure solution/refinement it soon turned out that the best and most stable refinements to the neutron diffraction data of LRAP_3 could be obtained with the *Pban* space group symmetry. Thus, we discuss this model within the main text. For this *Pban* model, during refinement of the 300 K data of sample LRAP_3, the occupation and the isotropic equivalent atomic displacement parameters for the hydrogen atoms were restrained to have the same values. They were similar in unconstraint refinements but caused some kind of instability and slow convergence. The data recorded at 4 K were treated similarly. Additionally, it was necessary here to restrain all the atomic displacement parameters for the Li atoms to have the same value. Adequately good results, based on reliability factors, were also possible with *Pmmm* symmetry, the structural data, obtained from the refinements on sample LRAP_3 are given in Table S3.

Table S4: Fractional atomic coordinates and equivalent isotropic atomic displacement parameters for $Li_2(OH)Cl$ (LRAP_3) in *Pmmm* symmetry, S.G. 47, at 300K (*a* =7.74898(10)Å, *b* = 8.00215(12) Å, *c* = 3.82511(5) Å, R_p = 10.8, R_{wp} = 7.40 and R_{Bragg} = 2.04) and 4 K (a = 7.69718(9) Å, *b* = 7.99502(2) Å, *c* = 3.77307(4) Å, R_p = 7.90, R_{wp} = 6.51 and R_{Bragg} = 1.57).

T = 300 K	Wyckoff	*x*	*y*	*z*	$B_{equ.}$	occ
Cl1	1*a*	0	0	0	1.62(14)	0.125
Cl2	1*b*	½	0	0	1.46(13)	0.125
Cl3	1*e*	0	½	0	2.48(14)	0.125
Cl4	1*f*	½	½	0	0.85(10)	0.125
O1	4*z*	0.2517(9)	0.2413(5)	½	1.29(4)	0.5
Li1	2*j*	0.248(5)	0	½	2.8(3)	0.25
Li2	2*l*	0.3077(18)	½	½	0.93(16)	0.25
Li3	2*p*	½	0.241(5)	½	3.9(4)	0.228(9)
Li4	4*y*	0.3178(12)	0.2189(18)	0	0.7(4)	0.263(12)
H1	8α	0.1974(20)	0.275(3)	0.288(4)	3.5(3)	0.253(4)
H2	8α	0.3185(21)	0.264(4)	0.362(4)	3.5(3)	0.253(4)
T = 4 K						
Cl1	1*a*	0	0	0	1.21(10)	0.125
Cl2	1*b*	½	0	0	1.05(10)	0.125
Cl3	1*e*	0	0.5	0	0.58(9)	0.125
Cl4	1*f*	½	½	0	2.76(16)	0.125
O1	4*z*	0.2521(8)	0.2426(8)	½	1.84(5)	0.5
Li1	2*j*	0.2129(23)	0	½	0.68(18)	0.25
Li2	2*l*	0.277(5)	0.5	½	3.7(2)	0.25
Li3	2*p*	½	0.247(6)	½	3.7(2)	0.219(7)
Li4	4*y*	0.3148(15)	0.239(5)	0	3.7(2)	0.255(9)
Li5	2*m*	0	0.283(3)	0	3.7(2)	0.154(7)
H1	8α	0.2133(12)	0.2840(12)	0.3128(22)	1.2(2)	0.222(3)
H2	8α	0.3389(11)	0.2630(24)	0.3852(22)	1.2(2)	0.222(3)

The two models are almost the same, the largest difference is a shift of the Cl atom into the origin to special positions 1*a* to 1*f* (Table S3). Close to the Li4 atom residual nuclear density was observed, which, however, could not be refined. This suggests a disorder of Li over two possible positions, which are close to each other. In the *Pban* model these two positions, over which Li seems to disorder, are related to each other by symmetry. Hence, they can be modelled properly. This is the main reason why the latter model is favoured over the other.

From inspection of the two "good working" models it is evident that O1 and Li1 atoms are displaced from each other along the **b** direction, thus they do not form a straight "line" along the **a** direction (marked by arrows in Figure S3). A similar behaviour is seen along the **a** direction with respect to O1 and Li2 atomic positions. Moreover, the Li3 atoms (for the the *Pban* model) are displaced also from special to more general positions and disordered. Taken together, this forces both the *a* and *b* unit cell dimensions to double; along *c* no such displacement is observed. From this structural evidence we conclude that the orthorhombic setting with the 2*a*, 2*b*, *c* cell setting *w.r.t.* the cubic parent cell is the most probable and correct one.

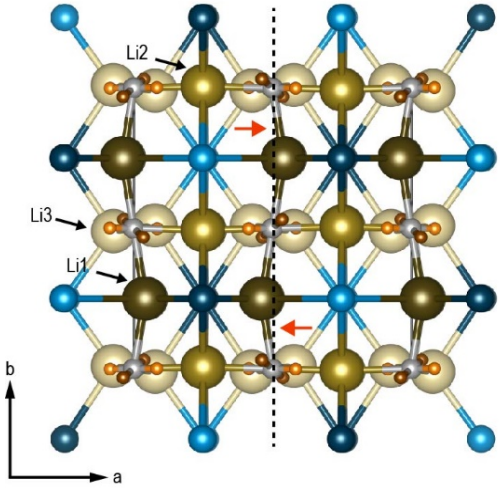

Figure S3: Structure of $Li_2(OH)Cl$ in the *Pban* symmetry in a projection along the *c*-axis. Illustration of the displacements of the Li1, Li2 and Li3 atoms forcing the doubling of *a* and *b* unit cell dimensions with respect to the cubic cell.

For all other space group symmetries, including *Cmcm*, (more) unstable refinements were obtained and *R*-values are distinctly larger. In particular, the Li and H positions could be identified from their negative nuclear densities in difference Fourier analysis. They could, however, could not be refined independently and the structural models partly differ distinctly depending on the refinement strategy. Some of the refinements do not properly converge.

Besides the main component $Li_2(OH)Cl$, the LRAP_3 sample, investigated by ND, contained small amounts of LiCl (9 wt. %). Despite the model used for $Li_2(OH)Cl$, and even if intensity should be allowed with the chosen space group symmetry (*e.g.*, in *Pban*, *Pmm2*, *Pmmm*, *Cmcm*), two reflections at 36.8° 2θ and 49.5° 2θ, respectively, could not be included in any of the refinements. They, however, can be matched with the unit cell parameters of the newly reported phase $LiCl \cdot 2\ H_2O$[20] although it was not possible to use the complete structural model of this compound. We assume that the impurity observed is $LiCl \cdot xH_2O$. It is similar, but structurally not exactly identical with the hydrate $LiCl \cdot 2H_2O$. This holds for both samples investigated. The hypothesis about an additional impurity, which arose during transport of the sample to the neutron source, is supported by the fact that in the samples that were characterized immediately after synthesis by XRD these reflections are absent, see Figure S4.

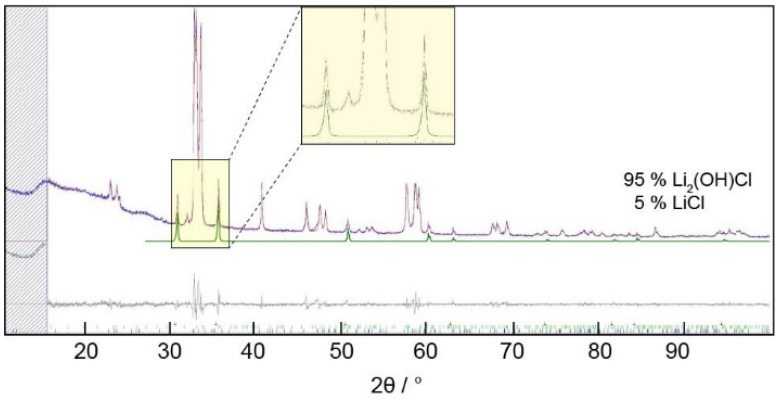

Figure S4: Result of the refinement of the LRAP_3 sample immediately after it has been synthesized.

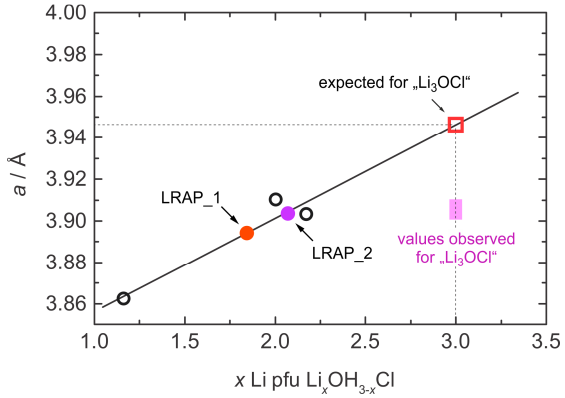

Figure S5. Experimentally probed lattice constant a of $Li_xOH_{3-x}Cl$ as a function of x Li per formula unit (pfu). For "Li_3OCl" one would expect $a \approx 3.95$ Å which has, to our knowledge, never been reported before by any structure refinement.[7,12]

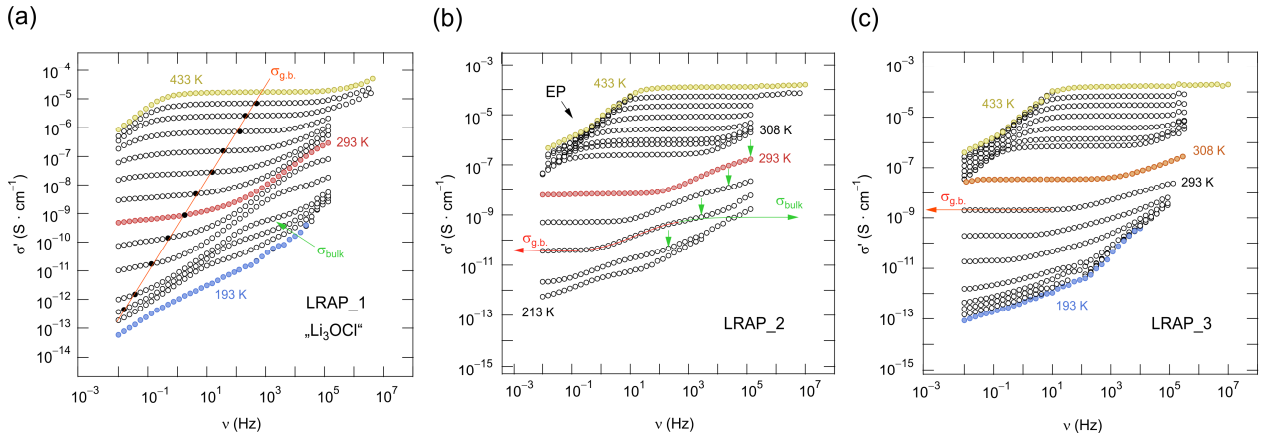

Figure S6: Conductivity isotherms of the hydrothermally synthesized samples LRAP_1 (a) and LRAP_2 (b). In (c) the electrical response of LiRAP_3 is shown that has been prepared via prepared via solid state reaction. Frequencies range from 10 mHz to 10 MHz; the measurements cover a temperature range from 193 K to 473 K in steps of 20 K. To monitor the change in impedance where the phase transition occurs additional isotherms were recorded at 208 K, 218 K, 308 K and 318 K. The broadband conductivity spectra of LRAP_1 and LRAP_2 exhibit two so-called frequency-independent plateaus. The first, seen at intermediate temperatures in the low frequency limit represent long-range ion transport which is usually identified as the direct current (dc) conductivity. Here, it represents the overall conductivity that is determined by the g.b. response; the solid line in (a) illustrates the change in σ_{dc} with temperature. With increasing frequency the dc-plateau of the isotherms passes into a dispersive region which finally reaches a second plateau, see the solid line in (b). From the saddle point seen we estimated bulk conductivities, *cf.* the vertical arrows. At even higher frequencies the isotherms reach the dispersive part of σ_{bulk}. In the ideal case the two plateaus correspond to two semicircles in the Nyquist ($-Z''$ vs. Z') representation, which yield $1/\sigma_{bulk}$ (and $1/\sigma_{g.b.}$) as the intercept with the Z' axis. The latter is only possible after appropriate simulation of the data in the complex plane representation with suitable equivalent circuits. As is well-known, this procedure is often fraught with difficulties since, as it is also in the present case, depressed, intertwined semicircles are obtained if correlation effects are present. Note that at the highest temperatures and the lowest frequencies ion transport is fast enough in order that the charge carriers pile up in front of the ion-blocking electrodes applied. Well-known electrode polarization (EP) causes σ' to decrease in this region, see (b).

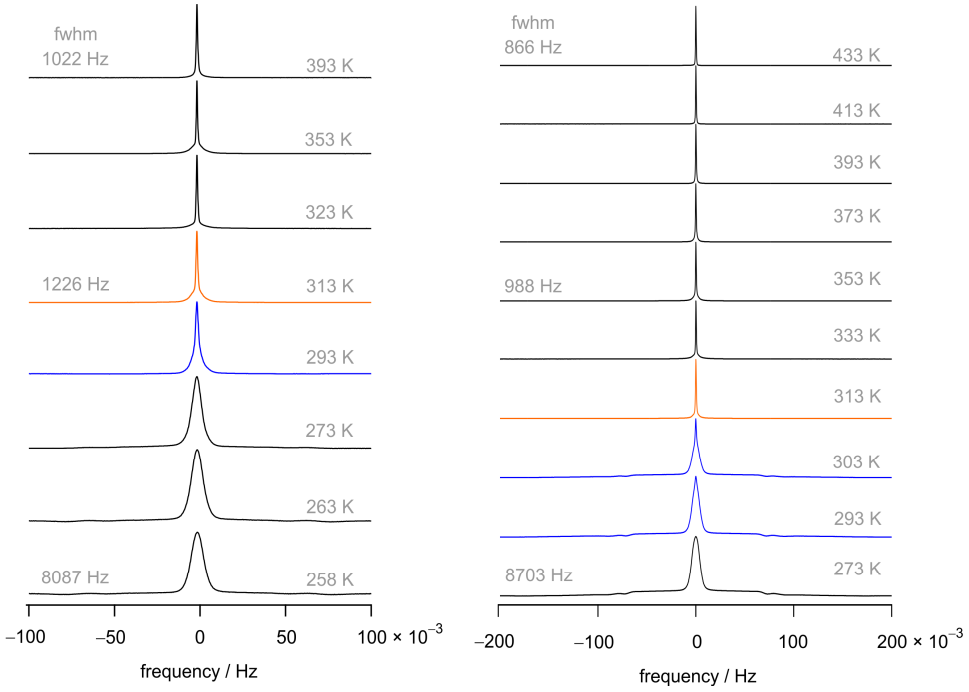

Figure S7: ^{7}Li NMR spectra of LiRAP_1 (left) and LiRAP_3 (right) recorded under static conditions at the temperatures indicated. At low *T* the central line is dipolarly broadened because of slow Li exchange. For LiRAP_3 we see a (first-order) quadrupole powder pattern as expected for a spin-3/2 nucleus such as ^{7}Li when the spin interacts with a non-vanishing electric field gradient. At ca. 300 K the line heterogeneously narrows indicating the phase transition from orthorhombic to cubic structure. A sharp NMR line is in agreement with Li ion exchange rates being sufficiently fast to average homonuclear dipole-dipole interactions. This observation is in agreement with the jump in electrical conductivity by 2-3 orders of magnitude, see Figure 5 c). A similar, but less pronounced, increase is seen for LiRAP_1. fwhm denotes full width at half maximum and illustrates the change in line width when going from very low to higher temperatures.

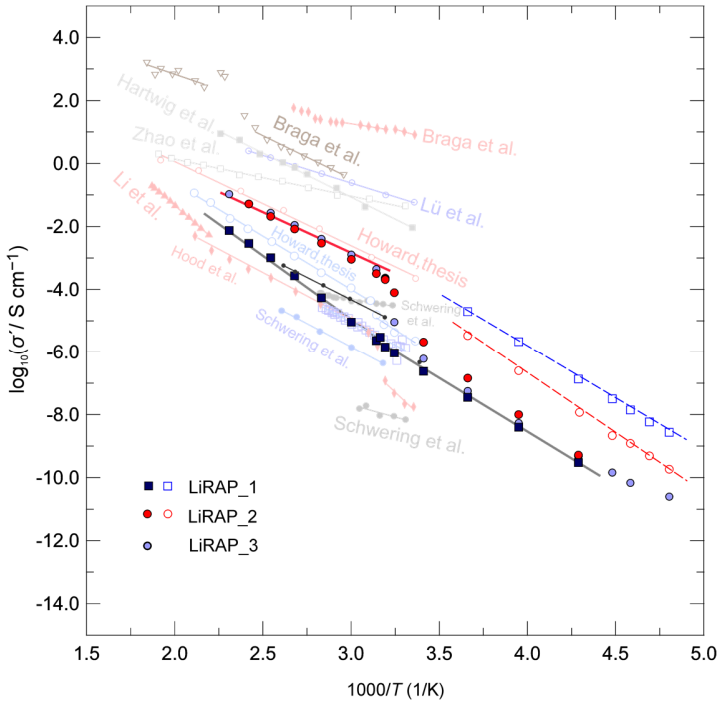

Figure S8: Comparison of conductivity data of the 3 samples investigated in this study with results presented in literature (see Refs. 5-8, 10-14). Here, the logarithm of the real part of the complex impedance σ is plotted as a function of the inverse temperature. Solid lines are to guide the eye.

References

(1) Scarpa G.; Atti R. Thermal analysis of the mixture of the alkali hydroxides with the corresponding halides. *Accad. Naz. Lincci, Sez. II*, **1915**, 24, 476.

(2) Reshcrnikov, N. A.; Unzhakov, G. M. Diagrammy plavkosti sistem LiOH-LiCl, LiOH-NaOH. *Zh. Neorg. Khim.* **1958**, 3, 1433.

(3) Berlange, H.; Jacobs, H.; Ungewöhnliche Koordinationspolyeder um Sauerstoff in $Li_4Cl(OH)_3$*Z. Anorg. Allg. Chem.,* **1994**, *620*, 471-474.

(4) Eilbracht, C.; Kockelmann, W.; Hohlwein, D.; Jacobs, H. *Proceedings of the First European Conference on Neutron Scattering. Phys. B*, **1997**, *234*, 48-50.

(5) Hood, Z. D., Wang, H.; Samuthira Pandian, A.; Keum, J. K. Liang, C. Li_2OHCl Crystalline electrolyte for stable metallic Lithium anodes. *J. Am. Chem. Soc.*, **2016**, *138*, 1768-1771.

(6) Howard, J.; Hood, Z. D.; Holzwarth, N. A. W. Fundamental aspects of the structural and electrolyte properties of Li_2OHCl from simulations and experiment. *Phys. Rev. Mater.,* **2017**, *1*, 075406.

(7) Li, Y.; Zhou, W.; Xin, S.; Li, S.; Zhu, J.; Lü, X.; Cui, Z.; Jia, Q.; Zhou, J.; Zhao, Y.; Goodenough, J. B Fluorine-doped anti-perovskite electrolyte for all-solid-state Lithium-ion batteries. *Angew. Chem. Int. Ed.*, **2016**, *128*, 9965-9968.

(8) Schwering, G.; Hönnerscheid, A.; van Wüllen, L.: Jansen, M. High Lithium ionic conductivity in the Lithium halide hydrates $Li_{3-n}(OH_n)Cl$ $(0.83 \leq n \leq 2)$ and $Li_{3-n}(OH_n)Br$ $(1 \leq n \leq 2)$ at ambient temperatures. *ChemPhysChem,* **2003**, *4*, 343-348.

(9) Hönnerscheid, A.; Nuss, J.; Mühle, C.; Jansen, M. Die Kristallstrukturen der Hydroxyhalogenide $Li_4(OH)_3Br$ und $Li_4(OH)_3I$. *Z. Anorg. Allg. Chem.,* **2003**, *629*, 312-316.

(10) Hartwig, P.; Rabenau, A.; Weppner, W. *J.* Lithium hydroxide halides: phase equilibria and ionic conductivities. *Less-Common Metals*, **1981**, *78*, 227-233.

(11) Zhao, Y.; Daemen, L. L. Superionic conductivity in Lithium-rich anti-perovskites. *J. Am. Chem. Soc.* **2012**, *134*, 15042-15047.

(12) Braga, M. H.; Ferreira, J. A.; Stockhausen, V.; Oliveirad J. E.; El-Azabe, A. Novel Li_3ClO based glasses with superionic properties for lithium batteries. *J. Mater. Chem. A*, **2014**, *2*, 5470-5480.

(13) Howard, J.W. Doctoral Dissertation (retrieved from ProQuest Dissertations and Theses. No. 3686123).

(14) Lü, X.; Wu, G..; Howard, J. W.; Chen, A.; Zhao, Y.; Daemen, L. L.; Jia, Q. Li-rich anti-perovskite Li_3OCl films with enhanced ionic conductivity. *Chem. Comm.* **2014**, *50*, 11520-11522.

(15) Altomare, A.; Cuocci, C.; Giacovazzo, C.; Moliterni, A.; Rizzi, R.; Corriero, N.; Falcicchio, A. A. EXPO2013: a kit of tools for phasing crystal structures from powder data. *J. Appl. Cryst.* **2013**, *46*, 1231-1235.

(16) Petříček, V.; Dusek, M.; Palatinus, L. Crystallographic Computing System JANA2006: General features. *Z. Kristallogr*. **2014**, *229*, 345-352.

(18) Song, A.-Y.; Xiao, Y.; Turcheniuk, K.; Upadhya, P.; Ramanujapuram, A.; Benson, J.; Magasinski, A.; Olguin, M.; Meda, L.; Borodin, O.; Yushin, G. Ion conductivities: Protons enhance conductivities in Lithium halide hydroxide/lithium oxyhalide solid electrolytes by forming rotating hydroxy groups. *Adv. Energy Mater.* **2018**, *8*, 1700971.

(19) Lerner; H.-W.; Bolte, M. An orthorhombic modification of lithium chloride monohydrate. *Acta Cryst. Sec. E* **2003**, *59*, i20-i21.

(20) Sohr, J.; Schmidt. H.; Voigt, W. Higher hydrates of lithium chloride, lithium bromide and lithium iodide. *Acta Cryst. Sec. C*, **2018**, *74*, 194-202.